

NUMERICAL SIMULATION OF THE FLOW OVER A CONFINED SHALLOW CAVITY

Thomas Emmert

Laboratoire de Mécanique des Structures Industrielles Durables,
UMR CNRS EDF 2832
1 avenue du Général de Gaulle, 92141 Clamart, France
thomas.emmert@edf.fr

Philippe Lafon

Laboratoire de Mécanique des Structures Industrielles Durables,
UMR CNRS EDF 2832
1 avenue du Général de Gaulle, 92141 Clamart, France
philippe.lafon@edf.fr

Christophe Bailly

Laboratoire de Mécanique des Fluides et d'Acoustique,
Ecole Centrale de Lyon & LMFA UMR CNRS 5509
36 avenue Guy de Collongue, 69134 Ecully, France
christophe.bailly@ec-lyon.fr

ABSTRACT

A high-Reynolds, moderate Mach number confined flow over a cavity is investigated numerically by solving the 3-D compressible Navier-Stokes equations with a high-order finite difference scheme. Experiments have shown that for some particular Mach number values of the flow above the cavity, a coupling occurs between the cavity flow and the pressure oscillations in the duct. Several simulations for different Mach numbers have been carried out in order to demonstrate the numerical coupling phenomena. The phase-locked frequencies are well predicted, but the oscillation amplitudes exhibit some differences.

INTRODUCTION

The configuration of the present ducted cavity has been first studied in the context of an industrial application (see Lafon *et al.* (2003)). Tonal noise has been measured on the power steam line of a nuclear power station and a cavity located in a gate valve has been identified as the noise source. This cavity has two specific characteristics that are different from classical cavities studied in the literature: it is confined and partially covered.

Confined cavities can not be only found in pipe systems with flow control devices but also in organ pipes or flutes for instance. They generate discrete tones that can be either disturbing when they excite the natural modes of the pipe structure or desirable for musical instruments. Like unconfined cavities, ducted cavities undergo a feedback mechanism that has been first described by Rossiter (1964): Vortical structures develop in the shear layer above the cavity and are convected downstream. The impact of the eddies on the downstream angle lead to pressure perturbations that trigger further instabilities at the upstream cavity angle resulting in phase-locked frequencies, called in the following cavity or Rossiter modes (RM).

For unconfined cavities, the oscillations remain weak for

flows at low Mach numbers. Most published papers therefore are addressed to cavity flows at the upper subsonic Mach numbers range (see Rockwell (1983); Shieh and Morris (2000); Gloerfelt *et al.* (2003)). For ducted cavities, the possible coupling between cavity oscillation modes and acoustic duct modes (DM) can however lead to high amplitude oscillations even at low speeds.

In the past many experimental and numerical investigations about unconfined cavities have been done, especially for predicting resonance frequencies and pressure levels (see Rockwell and Naudascher (1997); Gloerfelt *et al.* (2003); Rowley and Williams (2006)). The confined and partially covered cavity considered here has been already studied in 2-D by using a second-order TVD-Euler code (Lafon *et al.* (2003); Lafon and Devos (2003)). Rossiter frequencies have been recovered, but turbulent aspects could not be considered due to the inviscid 2-D simulation. A new numerical solver, called SAFARI (Simulation of Aeroacoustic Flows And Resonance and Interaction), has been developed to simulate aeroacoustic couplings for internal flows in complex geometries. In order to recover the interactions between the aerodynamic and acoustic field, compressible 3-D Navier-Stokes equations are solved using a high-order finite difference scheme. The experimental data are used to validate the numerical results. In particular the coupling between cavity modes and duct modes is considered.

The computational algorithm involving high-order numerical methods is reported in the first section. In the second section, the studied configuration is presented with emphasis on experimental results and physical mechanisms. In the third section, the simulation parameters are detailed and finally the results are analysed and commented in the last section.

NUMERICAL ALGORITHM

The set of equations are the compressible 3-D Navier-Stokes equations, written in conservative form after ap-

plication of a general time-invariant curvilinear coordinate transformation from physical space to computational space $(x, y, z) \rightarrow (\xi, \eta, \zeta)$. This yields

$$\frac{\partial}{\partial t} \left(\frac{\mathbf{Q}}{J} \right) + \frac{\partial \mathbf{E}}{\partial \xi} + \frac{\partial \mathbf{F}}{\partial \eta} + \frac{\partial \mathbf{G}}{\partial \zeta} = 0,$$

where J is the Jacobian of the geometric transformation. The unknown vector in the above equation writes $\mathbf{Q} = (\rho, \rho u, \rho v, \rho w, \rho e_t)^T$, where ρ designates the density, u, v, w the Cartesian velocity components and ρe_t the total energy. The latter is calculated for a perfect gas such as $\rho e_t = p/(\gamma - 1) + \rho(u^2 + v^2 + w^2)$ where p stands for the pressure. The flux vectors $\mathbf{E}, \mathbf{F}, \mathbf{G}$ contain the inviscid and the viscous terms. Their expressions as well as the metric identities for the grid transformation can be found in the work of Visbal and Gaitonde (2002) or Marsden *et al.* (2005). The viscosity is determined by Sutherland's law (Schlichting (1979)).

For interior points of the computational domain, the fluxes and the velocity derivatives for the viscous terms are discretized by the centered 11-point finite difference scheme developed by Bogey *et al.* (2004). This scheme has been optimized in wave number space and is able to resolve accurately perturbations with only four points per wavelength. An explicit fourth-order low-storage Runge-Kutta scheme advances the solution in time. An appropriate optimized explicit 11-point low pass filter remove grid-to-grid oscillations, not resolved by centered finite difference schemes (see Bogey *et al.* (2004)). At the same time the filter removes the non-resolved turbulent structures and acts like a sub-grid scale model. This method has been successfully applied by Bogey and Bailly (2006) and by Gaitonde and Visbal (2002). The filtering coefficient is chosen to be 0.2.

The implemented finite difference schemes are limited to structured grids. In order to treat more complex geometries, a high-order overset ability has been adapted and implemented in the code. In this approach the computational domain is subdivided into overlapping structured grid components. The governing equations are solved on each component grid separately and domain connectivity is obtained through the use of interpolation. Also known as the Chimera grid method, this approach has been first proposed by Benek *et al.* (1983) and extended for aeroacoustic simulations by Delfs (2001). For grid generation *ogen*, the grid assembler module of the freely available library *Overture* (see Henshaw (2007)) developed at the Lawrence Livermore National Laboratory, has been interfaced with the code. The conception of *Overture* as a library makes it easy to call grid assembler functions and makes the simulation of multiple bodies in relative motion and fluid structure interactions problems possible. For communication between grid boundaries that do not coincide, high-order interpolation is used. Lagrangian polynomials has been found by Sherer and Scott (2005) to be best suited in terms of precision, execution time and implementation aspects for the high-order overset grid approach. Various tests have shown that at least eight-order polynomials have to be used in order to make the error of the interpolation negligible when using the 11-points finite difference scheme.

For load balancing purpose, each component grid can be subdivided evenly N times in each direction and can be computed by $N_{\text{procs}} = N_{\xi, \text{procs}} \times N_{\eta, \text{procs}} \times N_{\zeta, \text{procs}}$. In a preprocessing step, SAFARI distributes the data concerning the computational grid and the interpolation provided by *ogen* for the parallel computation. The standard Message

Passing Interface (MPI) library routines have been used for code parallelization.

EXPERIMENTAL OBSERVATIONS

Due to the geometrical complexity of the cavity, a simplified plane model has been studied experimentally by Lafon *et al.* (2003). The retained geometry is reported in Figure 1.

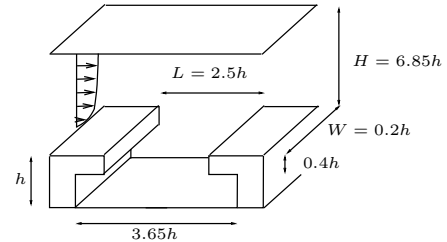


Figure 1: Ducted cavity: sketch of the geometry and notations $h = 0.02$ m, $d = 0.05$ m, $H = 0.137$ m, $L = 0.073$ m. U_0 is the free stream velocity considered as the nominal velocity, U_c is the convection velocity of eddies in the shear layer.

Details about the experiments are available in previous papers (see Lafon *et al.* (2003); Amandolese *et al.* (2002)). The main outlines are recalled here. The span of the test section has a value of 0.16 m. The reference pressure and density are given by $p_0 = 100000$ Pa and $\rho_0 = 1.2$ kg.m⁻³ respectively. Pressure signals have been measured by using a microphone located at the bottom center of the cavity. The measured spectra exhibit peaks that can be associated with the cavity modes. Plots of frequency and pressure level of these peaks as functions of the nominal Mach number $M_0 = U_0/c_0$, where c_0 denotes the sound velocity at reference conditions, are shown in Figure 2. Figure 3 shows corresponding plots of experimental Strouhal number compared to theoretical ones. The cavity modes can be estimated by Rossiter's formula (Rossiter (1964)):

$$St_R = f_R \frac{d}{U_0} = \frac{n_R - \xi}{M_0 + U_0/U_c},$$

where $\xi = 0.25$, $U_0/U_c = 0.57$, n_R is the mode number. They are plotted in Figure 3. The transverse duct modes are given by

$$St_d = f_d \frac{d}{U_0} = \frac{c}{2n_d H} \frac{d}{U_0},$$

where n_d is the mode number. The lock-in phenomenon can be observed when the frequencies of the cavity modes stops to scale with the theoretical RM evolution and continues to scale with the DM frequency. When lock-in occurs, the pressure level is maximum. This can be always observed when the RM approaches the DM. At $M = 0.13$, the 3. RM locks with the first DM and at $M = 0.18$, the 2. RM locks with the first DM. At $M = 0.23$, the 3. RM locks with the 2. DM. In this case the measured frequencies collapse with the 2. DM, based on the sum of the cavity and the duct height.

SIMULATION PARAMETERS

The entire overset grid generated by *ogen* is displayed in Figure 4. It consists of seven component grids. As the grid points of the communication interfaces coincide, no interpolation has to be used. The grid spacing is kept constant

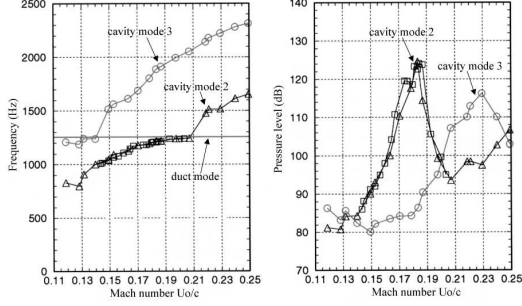


Figure 2: Frequency and level of pressure oscillations measured inside the cavity as functions of the Mach number.

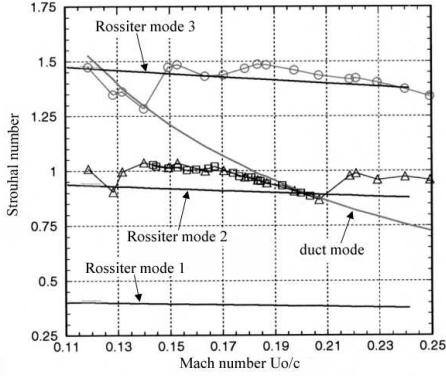


Figure 3: Strouhal number measured inside the cavity compared to theoretical ones as a function of the Mach number U_0/c_0 .

	N_x	N_y	N_z	N_{procs}
Duct	542	149	41	39
Neck	126	39	41	3
Cavity	180	61	41	5

Table 1: Grid parameters for the ducted cavity. The case has been computed by $N_{\text{procs}} = 47$ processors. The total number of grid points is 4×10^6 .

inside the cavity ($\Delta x = 4 \times 10^{-4}$ m and $\Delta y = 2 \times 10^{-4}$ m) and in the boundary layer ($\Delta y = 2 \times 10^{-4}$ m). In the duct, the grid is stretched in the y -direction near the upper wall with 3.0%. Upstream and downstream of the cavity the grid is stretched in the x -direction with 1.0%.

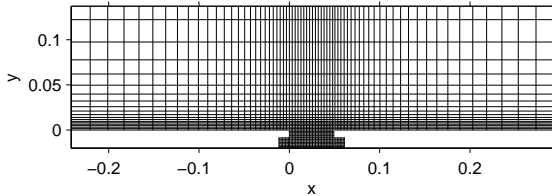


Figure 4: Overset grid generated by *ogen*. Every tenth line is represented.

The Reynolds number based on the duct height H and the velocity $U_0 = M_0 c_0$ is $Re_H \approx 5.6 \times 10^5$. The crucial point in cavity simulations is the boundary layer upstream the cavity, whose shape controls the vortex shedding and the convection of the eddies in the shear layer. The boundary layer profile that was measured experimentally is fitted by a $1/n$ profile (Schlichting (1979)) :

$$\frac{u_b(y)}{U_0} = \left(\frac{y}{\delta}\right)^{\frac{1}{n}},$$

where $\delta = 8.8$ mm and $n = 8.5$. The friction velocity is computed as $u_f = 2.65$ m/s gives a $\Delta y^+ = 23$. The boundary layer displacement thickness is $\delta_1 = 11$ mm. The Reynolds number based on δ_1 and $U_0 = 0.18c_0$ is thus $Re_{\delta_1} = 4398$. In order to avoid excessive filtering of the inflow velocity profile, only the fluctuating quantities are filtered. Upstream the cavity, the initial mean flow field is preserved during the simulation run.

As the flow Mach number lies in the low subsonic domain, the density and the pressure are taken constant over the whole height of the inflow and outflow ($p_{in} = p_{out} = 10^5$ N/m², $\rho_{in} = \rho_{out} = 1.2$ kg/m³). The inflow velocity profile, density and the pressure are imposed in a weak manner to prevent possible numerical drift. During the simulation they are recalled along the inlet boundary condition by a expression:

$$\tilde{\mathbf{Q}} = \mathbf{Q} - \sigma_{rc}(\mathbf{Q} - \mathbf{Q}_0),$$

where $\sigma_{rc} = 0.005$ has to be kept small in order to avoid numerical reflections. In a similar way, the pressure and the density at the outflow are recalled. A sponge zone combining grid stretching and a Laplacian filter at the outflow are used to avoid reflections.

By neglecting the influence of the boundary layer on the upper duct wall, slip conditions are applied. Otherwise no-slip adiabatic conditions have been implemented along the wall boundaries. In the spanwise direction, periodic conditions are applied.

RESULTS

Calculations have been carried out for several nominal Mach numbers M_0 : 0.13, 0.16, 0.18, 0.20, 0.21, 0.23 and 0.25. Figure 5 shows the iso-surface of a snapshot of the vorticity modulus inside the cavity obtained for $M_0 = 0.18$. The incoming boundary layer breaks down and generates coherent structures. Two coherent structures convecting in the shear layer can be observed and indicate the dominance of the second Rossiter's mode. Secondary longitudinal vortex rolls can be also observed.

The numerical spectra obtained from signals recorded at the bottom center of the cavity (as for the experiments) provides the frequency and the amplitude of the peaks associated with the second and third cavity modes. Figure 6 shows the evolution of the computed and measured frequencies of the modes. The frequency of the modes are well retrieved. At $M = 0.13$, lock-in between the 3. RM and the 1. DM, at $M = 0.20$, lock-in between the 2. RM and the 1. DM and at $M = 0.23$, lock-in between the 3. RM and the 2. DM occurs. In agreement with the experiments in the latter case, it is observed that the lock-in phenomenon occurs rather with the 2.DM mode based on the sum of the duct and cavity height.

Figure 7 shows the evolution of the computed and measured amplitudes of the cavity modes. The comparison is qualitatively good. The 2. RM remains too high after lock-in having occurred at $M = 0.20$. The amplitude of the 3. RM is overpredicted for low Mach numbers and underpredicted for higher Mach numbers. As a consequence, the crossing of the amplitude curves of the 2. RM and 3. RM at $M = 0.2$ is not reproduced and no dominance of the 3. RM can be detected.

Figures 8, 9, 10 show snapshots of the instantaneous pressure field in the duct and vorticity field in the cavity for three different Mach numbers $M_0 = 0.13, 0.20$ and 0.23 respectively. At $M = 0.20$, two eddies appear very distinctly

in the shear layer. This confirms the 2. RM to be dominant. In Figures 8 and 10, no dominant 3. RM can be detected, because for these two Mach numbers, the 2. RM and 3. RM have similar amplitudes. Preliminary 2-D computations using a similar grid resolution have overestimated the 2. RM. For the 2-D case this has been caused by an over prediction of the recirculation zone inside the cavity due to the absence of 3-D mixing. This indicates that the size in spanwise direction is too small and 2-D effects seem to play a role.

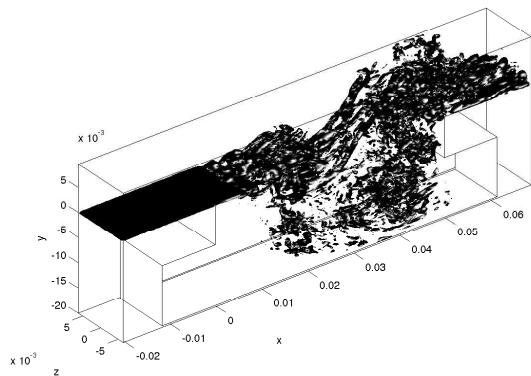


Figure 5: Computed instantaneous vorticity modulus field ($|\omega| = 25 \times 10^3 \text{s}^{-1}$) for $M_0 = 0.13$.

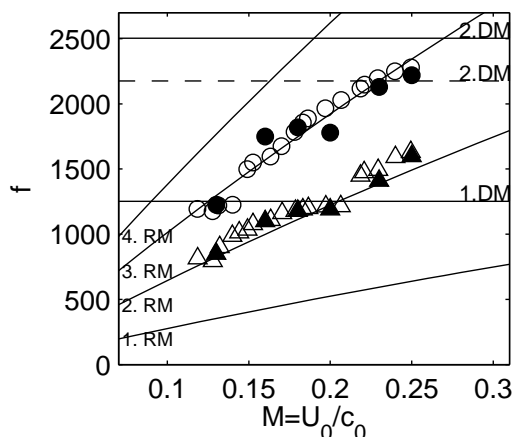


Figure 6: Computed frequencies (\blacktriangle mode 2, \bullet mode 3) of the cavity modes compared to experimental ones (\triangle mode 2, \circ mode 3) and to Rossiter's and duct mode frequencies (RM = Rossiter's mode, DM = duct modes). The modified 2.DM mode is calculated with the sum of the duct and the cavity heights.

CONCLUSION

The present study shows the feasibility to reproduce the coupling lock-in phenomenon between the cavity modes and the duct modes with the present numerical algorithm. Qualitative discrepancies, in particular the absence of a dominant 3. cavity mode, are currently under examination. Grid convergence studies and computations taking into account the lateral walls of the cavity are currently in work. The implementation of a realistic turbulent boundary layer as the inflow condition are planned in the future.

ACKNOWLEDGMENTS

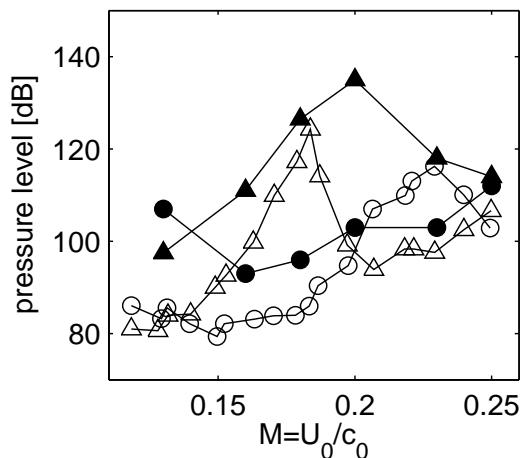


Figure 7: Computed power levels (\blacktriangle mode 2, \bullet mode 3) of the cavity modes compared to experimental ones (\triangle mode 2, \circ , mode 3).

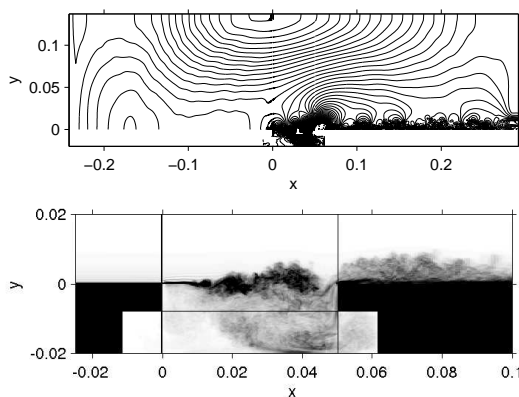


Figure 8: Computed instantaneous results for $M_0 = 0.13$. Top: pressure fluctuations (< 200 Pa) in the duct. Bottom: spanwise averaged vorticity modulus in the cavity.

Thanks to William Henshaw (Lawrence Livermore National Laboratory) for providing useful advices about the *Overture* library.

REFERENCES

- Amandolese, X., Hemon, P., and REGARDIN, C., 2002, "Study of the acoustic oscillations by flows over cavities", *Proceedings of the Fifth International Symposium on Fluid-Structure Interactions, IMECE'02*, New Orleans.
- Benek, J. A., Steger, J.L., and Dougherty, F. C., 1983, "A flexible grid embedding technique with applications to the Euler equations", AIAA Paper 83-1944.
- Bogey, C., and Bailly, C., 2002, "Three dimensional non-reflective boundary conditions for acoustic simulation: far field formulation and validation test cases", *Acta Acustica United with Acustica*, Vol. 88, pp. 463-471.
- Bogey, C., Bailly, C., and Juve, D., 2002, "A family of low dispersive and low dissipative schemes for Large Eddy Simulations and for sound propagation", *Journal of Computational Physics*, Vol. 194, pp. 194-214.

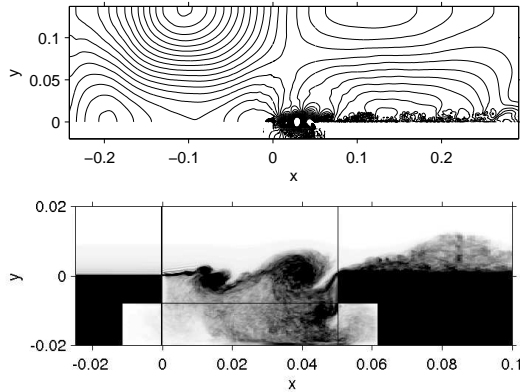


Figure 9: Computed instantaneous results for $M_0 = 0.20$. Top: pressure fluctuations (< 200 Pa) in the duct. Bottom: spanwise averaged vorticity modulus in the cavity.

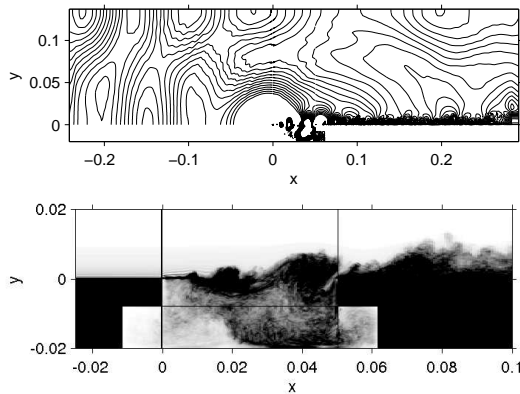


Figure 10: Computed instantaneous results for $M_0 = 0.25$. Top: pressure fluctuations (< 100 Pa) in the duct. Bottom: spanwise averaged vorticity modulus in the cavity.

Bogey, C., and Bailly, C., 2006, "Large Eddy Simulations of transitional round jets : influence of the Reynolds number on flow development and energy dissipation", *Physics of Fluids*, Vol. 18, pp. 1-14.

Delfs, J. W., 2001, "An overlapped grid technique for high resolution CAA schemes for complex geometries", AIAA Paper 2001-2199.

Gaitonde, D. V., and Visbal, M. R., 2002, "Advances in the application of high-order techniques in simulation of multi-disciplinary phenomena ", *International Journal of Computational Fluid Dynamics*, Vol. 17, pp. 95-106.

Gloerfelt, X., Bailly, C., and Juve, D., 2003, "Direct computation of the noise radiated by a subsonic cavity flow and application of integral methods", *Journal of Sound and Vibration*, Vol. 266, pp. 119-146.

Gloerfelt, X., Bogey, C., and Bailly, C., 2003, "Numerical evidence of mode switching in the flow-induced oscillations by a cavity", *Int. J. of Aeroacoustics*, Vol. 2, pp. 99-124.

Henshaw, W. D., 2007, "Ogen: an overlapping grid generator for Overture", <http://www.llnl.gov/casc/Overture>.

Lafon, P., Caillaud, S., Devos, J. P., and Lambert, C., 2003, "Aeroacoustical coupling in a ducted shallow cavity

and fluid-structure effects on a steam line", *Journal of Fluids and Structures*, Vol. 18, pp. 695-713.

Lafon, P., and Devos, J. P., 2003, "Computation of the noise generated by a shallow cavity and test of a solution for lowering the noise", AIAA Paper 2003-3105.

Marsden, O., Bogey, C., and Bailly, C., 2005, "High-order curvilinear simulations of flows around non-cartesian bodies", *Journal of Computational Acoustics*, Vol. 13, pp. 732-748.

Rockwell, D., 1983, "Oscillations of impinging shear layers", *AIAA Journal*, Vol. 21, pp. 645-664.

Rockwell, D., and Naudascher, E., 1997, "Self-sustained oscillations of impinging free shear layer", *Annual Review of Fluid Mechanics*, Vol. 11, pp. 67-94.

Rossiter C. W., 1964, "Wind-tunnel experiments in the flow over rectangular cavities at subsonic and transonic speeds", Aeronautical Research Council Reports and Memoranda, Technical Report 3438.

Rowley, C. W., and Williams, D. R., 2006, "Dynamics and control of high-Reynolds number flow over open cavities", *Annual Review of Fluid Mechanics*, Vol. 38, pp. 251-276.

Schlichting H., 1979, "Boundary Layer Theory", McGraw-Hill, Inc.

Sherer, S. E., and Scott, J. N., 2005, "High-order compact finite-difference methods on general overset grids", *Journal of Computational Physics*, Vol. 210, pp. 459-496.

Shieh, C. M., and Morris, P. J., 2000, "Parallel computational aeroacoustic simulation of turbulent subsonic cavity flow", AIAA Paper 2000-1914.

Tam, C. K. W., and Dong, Z., (1996), "Radiation and out-flow boundary conditions for direct computation of acoustic and flow disturbances in a nonuniform mean flow", *Journal of Computational Acoustics*, Vol. 4, pp. 175-201.

Visbal, M. R., and Gaitonde, D. V., 2002, "On the use of higher-order finite-difference schemes on curvilinear and deforming meshes", *Journal of Computational Physics*, Vol. 181, pp. 155-185.

